

# Experimental and numerical analyses of carbon tetrachloride under laser-driven shock compression

Eisuke Yamada<sup>\*†</sup>, Kunihiro Wakabayashi<sup>\*\*</sup>, and Mitsuo Koshi<sup>\*\*\*</sup>

<sup>\*</sup>College of Science and Engineering, Aoyama Gakuin University, 5-10-1 Fuchinobe, Sagamihara, Kanagawa 229-8558, JAPAN

<sup>†</sup>Corresponding address: yamada@me.aoyama.ac.jp

<sup>\*\*</sup>Research Core for Explosion Safety, National Institute of Advanced Industrial Science and Technology (AIST), Central 5, 1-1-1 Higashi, Tsukuba, Ibaraki 305-8565, JAPAN

<sup>\*\*\*</sup>Graduate School of Engineering, The University of Tokyo, 7-3-1 Hongo, Bunkyo-Ku, Tokyo 113-8656, JAPAN

Received: January 23, 2008 Accepted: April 2, 2008

## Abstract

Raman spectroscopy has been applied to carbon tetrachloride under the laser-driven shock compression. Compressed area and the area that has still not been compressed coexist in the carbon tetrachloride, when the shock wave passes. Therefore, obtained Raman spectrum consists of two areas. In order to discuss the areas in detail, numerical simulation based on the compressible fluid dynamics has been applied. Although the effect of rarefaction wave is not considered, this numerical simulation provides a reasonable result for the early stage of the shock compression.

**Keywords:** Carbon tetrachloride, Compressible flow, Condensed matter, Shock wave.

## 1. Introduction

Recently, laser-driven shock compression method is often used to explore the physical properties of a substance under the shock compression<sup>1)-4)</sup>. A pulsed laser easily induces extremely high pressure and high density in a micro space. Raman spectroscopy is usually applied to investigate a change of molecular mechanism under the shock compression. Analyses of Raman spectrum from a compressed matter indicate the phase transition and the change of temperature under the high pressure<sup>5)-7)</sup>.

A shock wave induced by a pulsed laser traverses very rapidly. When the shock wave traverses in a material, compressed area and the area that has still not been compressed coexist in the material. Figure 1 shows a typical condition of shock wave and a measurement of Raman spectrum under the laser-driven shock compression. The pulsed laser from the left-hand side enters the aluminum wall, and an ablation of the aluminum is occurred. Part of the aluminum wall penetrates to the material, and the shock wave makes progress toward the right-hand side. While, the pulsed laser for Raman probe enters it from the opposite side. Obtained Raman spectrum of the mate-

rial like a colorless liquid is superimposed spectrum of compressed area and the area that has still not been compressed. Raman spectrum split in two presents Raman shift induced by high pressure. Comparing the intensity of Stokes and anti-Stokes peak, shock temperature was

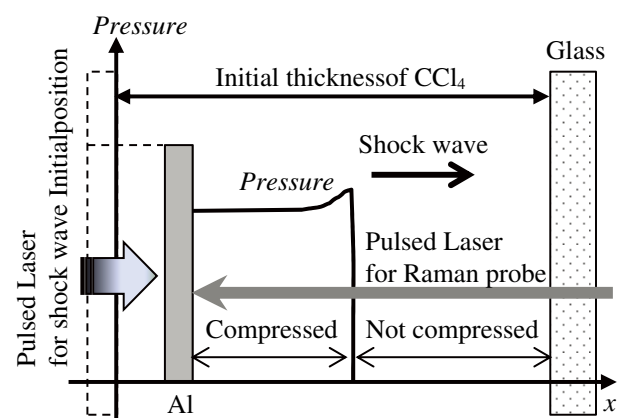


Fig. 1 Typical condition of shock wave and a measurement of Raman spectrum under the laser-driven shock compression.

estimated. However, it is quite difficult to measure a spatial distribution of temperature at a certain time, since this phenomenon is finished very fast in the limited slight space. Therefore, numerical simulation based on the compressible fluid dynamics has been applied to estimate spatial distributions of temperature at a certain time.

In this study, carbon tetrachloride ( $\text{CCl}_4$ ) has used as a sample material, since the properties of liquid  $\text{CCl}_4$  under the shock compression is well-known experimentally<sup>8)-10)</sup>.  $\text{CCl}_4$  has intense Raman bands at relatively low energies. It is convenient to determine a shock temperature with Raman spectrometry. A moving boundary condition for the numerical simulation was measured by laser interferometer. Comparing the results of numerical simulation with the results of Raman spectrometry, the effects of compressed area and the area that has still not been compressed at a certain time are clearly.

## 2. Experimental method

Two Q-switched Nd<sup>3+</sup>:YAG lasers were used for pump and probe experiments. One was used as a pump laser (Continuum, Inc., YG2671-10) for the irradiation of the target, which generates shock waves. The other one was used as a probe laser (Continuum, Inc., Minilite) for the excitation of Raman scattering. Wavelength and pulse width was 1064 nm and 10 ns for the pump laser, and 532 nm and 5.5 ns for the probe laser, respectively. Temporal profile of lasers was near-Gaussian.

The target assembly has a glass confinement geometry<sup>11)</sup>, which consists of a back-up glass (BK7, 50 × 50 × 3 mm<sup>3</sup>), an aluminum foil (Nilaco Co., 25 μm thick), polytetrafluoroethylene-spacers (Nilaco Co., 185 μm thick) and a cover glass (BK7, 50 × 50 × 3 mm<sup>3</sup>). The aluminum foil was glued on the back-up glass with ultraviolet cure adhesive. Carbon tetrachloride was filled between two glass plates.

The pump laser was focused on the aluminum foil through a back-up glass with a spot (approximately 0.5 mm<sup>2</sup>). Laser induced plasma was generated at the interface between aluminum and back-up glass, and drove a shock wave through the aluminum foil into the carbon tetrachloride. Micro lens array (advanced microoptical systems GmbH, ANH-Q-P1000-R91) was used to homogenize intensity distribution of the pump laser, and to generate shock wave with flat shock front.

The probe laser was focused on the rear side of the target with a diameter of 500 μm. The energy of the probe laser was 0.5 ~ 1.0 mJ / pulse. Raman scattered light was collected with a camera lens, and introduced to the spectrometer (Kaiser optical systems, Inc., HoloSpec f / 1.8 i) by an optical fiber with 200 μm core. Two notch filters (Kaiser optical systems, Inc.) were used for rejection of Rayleigh scattered light. Spectrally resolved light was detected by the intensified CCD camera (Andor Technology, DH720-18F-73). Lasers and ICCD camera were synchronized by the use of the digital delay pulse generators (Berkeley Nucleonics Co., Ltd., BNC555). Raman spectrum was obtained by single shot experiment.

## 3. Numerical simulation

The phenomenon considered in this study is finished very fast in a limited slight space. The shock wave virtually propagates straight. Therefore, 1-dimensional simulation is enough to analyze this phenomenon.

Conservation equations are assumed as follows.

$$\frac{\partial \rho}{\partial t} + u \frac{\partial \rho}{\partial x} = -\rho \frac{\partial u}{\partial x} \quad (1)$$

$$\frac{\partial u}{\partial t} + u \frac{\partial u}{\partial x} = -\frac{1}{\rho} \frac{\partial p}{\partial x} \quad (2)$$

$$\frac{\partial e}{\partial t} + u \frac{\partial e}{\partial x} = -\frac{p}{\rho} \frac{\partial u}{\partial x} \quad (3)$$

Where  $\rho$  is the density,  $t$  is the time,  $u$  is the velocity,  $x$  is the coordinate,  $p$  is the pressure, and  $e$  is the energy per unit mass. These are typical equations based on the compressible fluid dynamics. Equations (1)-(3) were made in discrete forms, and CIP scheme was applied<sup>12)</sup>.

In order to estimate the pressure, equation of state is defined by Hugoniot empirical equation

$$p = p_0 + \rho u (C + Su) \quad (4)$$

where  $p_0$  is the initial pressure,  $C$  and  $S$  are the constants. For carbon tetrachloride,  $C$  and  $S$  are defined to 1.11 and 1.67, respectively<sup>13)</sup>.

Figure 2 shows the analytical model of the numerical simulation. The initial length of calculation domain is 200 μm according to the experimental configuration. There are 1001 grid points for calculation with mesh width of 0.2 μm. Pulsed laser pushes the wall, and then shock wave enters the carbon tetrachloride. Some initial conditions are described in Fig. 2.

The moving velocity of the wall was measured by the laser interferometer. Figure 3 shows the interference pattern at pulsed laser energy 115 mJ on the target. This image consists of 512 × 512 pixel taken by the streak camera (Hamamatsu Photonics:C5680). Slit size of this camera is 50 μm. Time direction is downward with 200 ns recording time. To define the time when the wall starts to move, Rayleigh scattering from the pulsed laser for Raman probe was detected. This signal was analyzed, and then 98th pixel line from top of the image was defined to

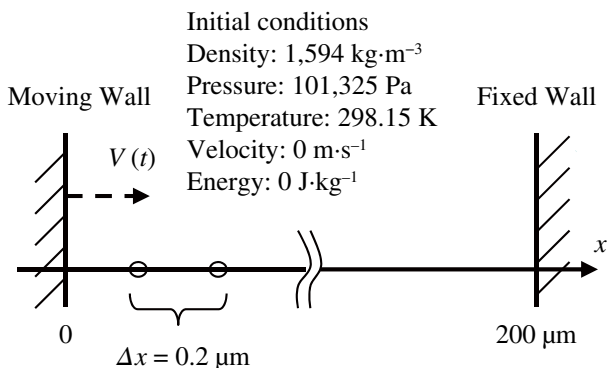


Fig. 2 Analytical model and boundary conditions for the numerical simulation.

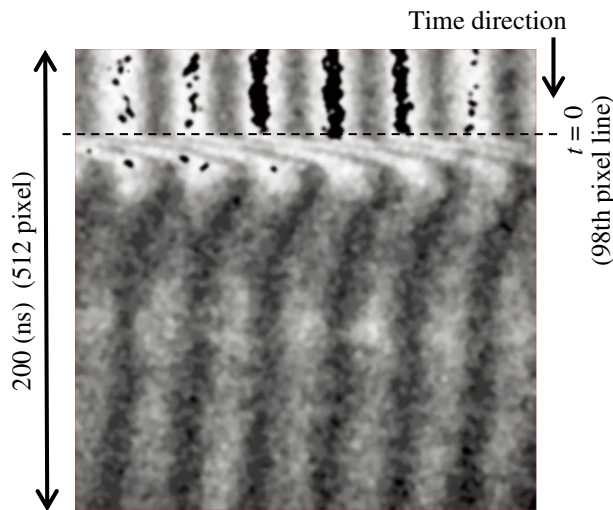


Fig. 3 Interference pattern ( $512 \times 512$  pixel) measured by the laser interferometer system. Laser energy for the shock wave is 115 mJ on the target.

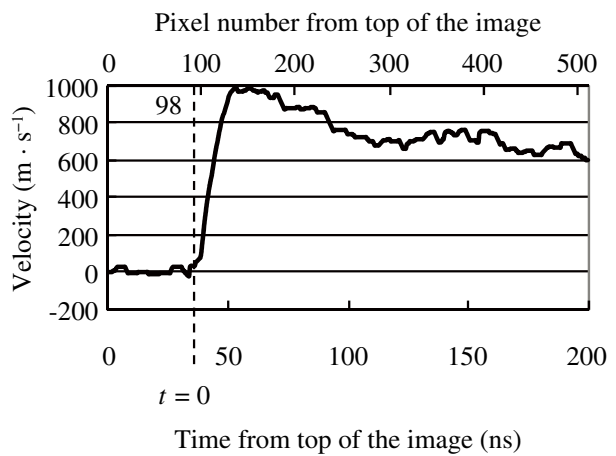


Fig. 4 Velocity change of the moving aluminum wall estimated by the laser interferogram shown in Fig. 3.

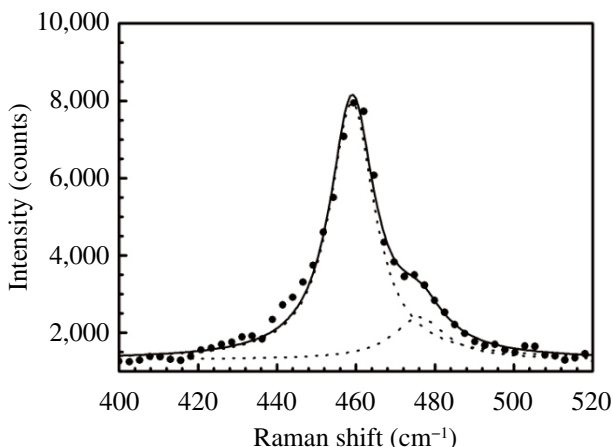


Fig. 5 Raman shift intensity at 15 ns in Stokes region around  $460 \text{ cm}^{-1}$ . Experimental data (circles), fits to the modes (dashed lines) and sum of the fits (solid line).

$t = 0$ , i. e., it is the time when the wall starts to move.

Figure 4 shows the velocity change of the wall, which was obtained by analysis of the laser interferogram shown in Fig. 3. This temporal change of velocity was used as a moving boundary condition of the numerical simulation.

Additionally, following equation is used to estimate temperature  $T$ .

$$\int_{T_r}^T C_v dT = e - e_r \quad (5)$$

Where  $C_v$  is the specific heat at constant volume.  $T_r$  and  $e_r$  are reference temperature and reference energy, respectively. In this study, these are initial temperature and initial energy. Absolute value of the energy is not important to estimate the temperature with eq. (5). Difference of the energy is an essential. Therefore, the initial energy was defined as zero.  $C_v$  for  $\text{CCl}_4$  depends on the temperature as follows<sup>14)</sup>.

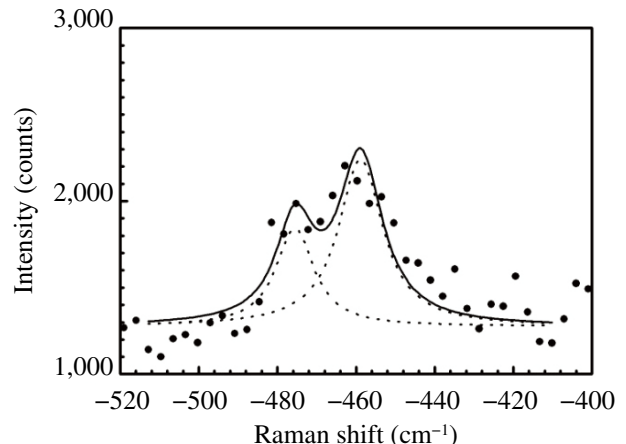


Fig. 6 Raman shift intensity at 15 ns in anti-Stokes region around  $-460 \text{ cm}^{-1}$ . Experimental data (circles), fits to the modes (dashed lines) and sum of the fits (solid line).

$$C_v(T) = A + \frac{B}{T^2} + \frac{C}{T} + D + ET + FT^2 [\text{cal} \cdot \text{mol}^{-1} \cdot \text{K}^{-1}] \quad (6)$$

$$A = 21.7, B = -75415.8, C = -2109.31, D = 8.10247, E = -8.64548 \times 10^{-4}, F = 1.12516 \times 10^{-7}$$

With eqs. (1) ~ (6), the spatial distributions of pressure and temperature can be calculated.

#### 4. Results and discussion

Figures 5 and 6 show the obtained Raman peak at  $459 \text{ cm}^{-1}$  mode in the Stokes and anti-Stokes region, respectively. These spectra were obtained at 15 ns after the shock enters the  $\text{CCl}_4$ . These distributions are fitted by Lorentz functions to separate into two peaks. The peak of  $\pm 459 \text{ cm}^{-1}$  is well-known intense Raman bands of  $\text{CCl}_4$  under the room temperature and pressure. Other peak of  $\pm 476 \text{ cm}^{-1}$  is induced by the shock compression. Comparing the intensity of Stokes and anti-Stokes peak in  $\pm 475 \text{ cm}^{-1}$ ,  $773 \pm 92 \text{ K}$  was estimated as the shock temperature<sup>8)</sup>.

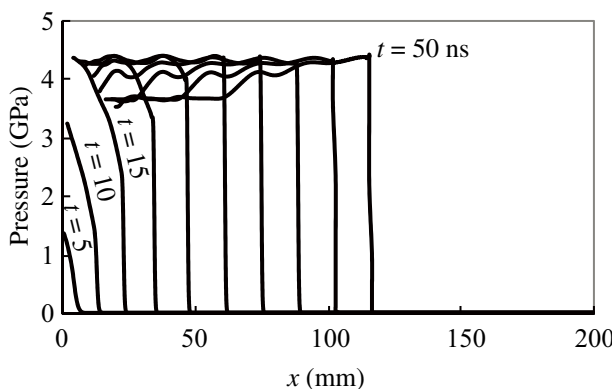


Fig. 7 Spatial distributions of the pressure at each 5 ns.

Table 1 Mean temperature at 15 ns classified by the lower limit of pressure.

lower limit of pressure (GPa)	Range (mm)	mean temperature (K)
0.5	4.4 – 23.6	720
1.0	4.4 – 23.4	724
1.5	4.4 – 23.2	728
2.0	4.4 – 23.0	732
2.5	4.4 – 22.0	742
3.0	4.4 – 19.6	762
3.5	4.4 – 16.0	790
4.0	4.4 – 11.2	842

Figures 7 and 8 are results of the numerical simulation, which show the spatial distributions of pressure and temperature at each 5 ns, respectively. The shock wave enters from the left-hand side, and the pressure increases up to 4 GPa by 15 ns. Afterward, the shock wave propagates to the right-hand side with a constant velocity. At 15 ns, the shock front reaches ca. 23.6 μm, and moving wall is shifted to ca. 4.4 μm from the initial position. Mean temperature is 720 K in this region. This calculated temperature is slightly lower than the temperature estimated by Raman spectroscopy.

Distance between Raman shift peaks usually depends on the scale of pressure. Higher pressure causes a new peak at a position more away from the peak under the atmospheric pressure. The peak of  $\pm 475 \text{ cm}^{-1}$  shown in Figs. 5 and 6 is mainly induced by a certain high pressure. Table 1 lists a mean temperature at 15 ns obtained by the numerical simulation. Each range is limited by a lower limit of pressure. When the lower limit of pressure is 3.0 GPa, mean temperature is 762 K. Accordingly, it is found that the observed Raman shift of  $475 \text{ cm}^{-1}$  at 15 ns was mainly induced by the pressure over 3.0 GPa.

However, rarefaction wave enters behind the shock wave from the side of the compressed volume. Although the effect of rarefaction was neglect, the numerical simulation provides a reasonable result for the early stage of the shock compression. When the shock wave reaches more far away, it is found that this effect becomes larger behind the shock wave. Therefore, it is need to consider the rarefaction wave in the numerical simulation properly.

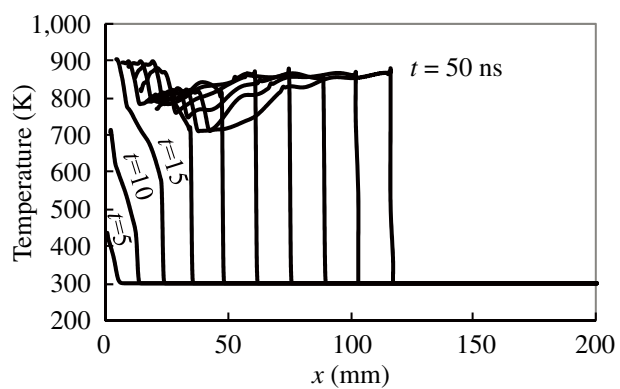


Fig. 8 Spatial distributions of the temperature at each 5 ns.

## 5. Conclusions

In this study, shock temperature of carbon tetrachloride is compared between the experimental result and numerical simulation. At 15 ns after the shock wave reaches carbon tetrachloride, we concluded that this shock temperature was mainly induced by the pressure over 3.0 GPa.

The effect of rarefaction was not considered in this numerical simulation. For the early stage of the shock compression, however, this numerical simulation established a new meaningful result from Raman spectrometry. For the other materials, this method can be also applied to understand the phenomena under the shock compression.

## Acknowledgment

This work was supported by the Ministry of Education, Culture, Sports, Science, and Technology of Japan (Monbu-Kagaku-Sho).

## References

- 1) G. Tas, S. A. Hambir, J. Franken, D. E. Hare, D. D. Dlott, *J. Appl. Phys.*, 82, 1080 (1997).
- 2) D. D. Dlott, S. Hambir, J. Franken, *J. Phys. Chem. B*, 102, 2121 (1998).
- 3) H. He, T. Kobayashi, T. Sekine, *Rev. Sci. Instrum.* 72, 2032 (2001).
- 4) S. D. McGrane, D. S. Moore, D. J. Funk, *J. Phys. Chem. A*, 108, 9342 (2004).
- 5) D. D. Dlott, *Accounts Chem. Res.*, 33, 37 (2000).
- 6) A. Matsuda, H. Nagao, K. G. Nakamura, K. Kondo, *Chem. Phys. Lett.*, 372, 911 (2003).
- 7) A. Matsuda, K. Kondo, K. G. Nakamura, *J. Chem. Phys.*, 124, 054501 (2006).
- 8) G. I. Pangilinan, Y. M. Gupta, *J. Appl. Phys.*, 81, 6662 (1997).
- 9) O. V. Fat'yanov, T. Ogura, M. F. Nicol, K. G. Nakamura, K. Kondo, *Appl. Phys. Lett.*, 77, 960 (2000).
- 10) H. Kawamura, M. Kobayashi, Y. Yamamoto, N. Matsui, Y. Akahama, *Solid State Commun.*, 102, 501 (1997).
- 11) D. Devaux, R. Fabbro, L. Tollier, and E. Bartnicki, *J. Appl. Phys.*, 74, 2268 (1993).
- 12) T. Yabe, T. Aoki, *Comput. Phys. Commun.*, 66, 219 (1991).
- 13) R. D. Dick, *J. Chem. Phys.*, 52, 6021 (1970).
- 14) M. Cowperthwaite, R. Shaw, *J. Chem. Phys.*, 53, 555 (1970).

# レーザーショック法により圧縮された四塩化炭素の実験 および数値計算による解析

山田英助 \*†, 若林邦彦 \*\*, 越 光男 \*\*\*

レーザーショック法により四塩化炭素の動的圧縮実験を行い、四塩化炭素からのラマン散乱光の変化を観測した。衝撃波が伝播している時、四塩化炭素には空間的に圧縮された領域と非圧縮の領域が共存している。観測されたラマン散乱光は、この二つの領域の影響が重ね合わさったものである。この領域を詳細に議論するために、圧縮性流体力学に基づく数値シミュレーションを行った。希薄波の影響は加味していないが、レーザーショックの初期段階においては、数値シミュレーションから妥当な結果が得られた。

\*青山学院大学理工学部 〒229-8558 神奈川県相模原市淵野辺5-10-1

†Corresponding address: yamada@me.aoyama.ac.jp

\*\*産業技術総合研究所 〒305-8565 茨城県つくば市東1-1-1

\*\*\*東京大学大学院工学系研究科 〒113-8656 東京都文京区本郷7-3-1